

OncoNetExplainer: Explainable Predictions of Cancer Types Based on Gene Expression Data

Md. Rezaul Karim^{*†}, Michael Cochez[‡], Oya Beyan^{†*}, Stefan Decker^{†*}, and Christoph Lange^{*†}

^{*} Fraunhofer Institute for Applied Information Technology FIT, Germany

[†] Information Systems and Databases, RWTH Aachen University, Germany

[‡] Department of Computer Science, Vrije Universiteit Amsterdam, the Netherlands

Abstract—The discovery of important biomarkers is a significant step towards understanding the molecular mechanisms of carcinogenesis; enabling accurate diagnosis for, and prognosis of, a certain cancer type. Before recommending any diagnosis, genomics data such as gene expressions (GE) and clinical outcomes need to be analyzed. However, complex nature, high dimensionality, and heterogeneity in genomics data make the overall analysis challenging. Convolutional neural networks (CNN) have shown tremendous success in solving such problems. However, neural network models are perceived mostly as ‘black box’ methods because of their not well-understood internal functioning. However, interpretability is important to provide insights on why a given cancer case has a certain type. Besides, finding the most important biomarkers can help in recommending more accurate treatments and drug repositioning. Moreover, the ‘right to explanation’ of the EU GDPR gives patients the right to know why and how an algorithm made a diagnosis decision. Hence, in this paper, we propose a new approach called *OncoNetExplainer* to make explainable predictions of cancer types based on GE data. We used genomics data about 9,074 cancer patients covering 33 different cancer types from the Pan-Cancer Atlas on which we trained CNN and VGG16 networks using guided-gradient class activation maps++ (GradCAM++). Further, we generate class-specific heat maps to identify significant biomarkers and computed feature importance in terms of mean absolute impact to rank top genes across all the cancer types. Quantitative and qualitative analyses show that both models exhibit high confidence at predicting the cancer types correctly giving an average precision of 96.25%. To provide comparisons with the baselines, we identified top genes, and cancer-specific driver genes using gradient boosted trees and SHapley Additive Explanations (SHAP). Finally, our findings were validated with the annotations provided by the TumorPortal.

Index Terms—Cancer genomics, Gene expression, Neural networks, GradCAM++, Interpretability, Explainable AI.

I. INTRODUCTION

Cancer is caused by gene alterations and abnormal behaviors of genes that control cell division and cell growth. The change in the structure of occurring genetic aberrations, such as somatic mutations, copy number variations (CNV), profiles, and different epigenetic alterations are unique for each type of cancer [1,2]. As a result, gene expressions (GE) can be disrupted by cell division or environmental effects, or genetically inherited from parents. Changes in GE sometimes change the production of different proteins, affecting normal cell behavior. These damaged cells start reproducing more rapidly than usual and gradually increase in the affected area by forming a tumor. Intermittently, such tumors turn into a type of cancer [3,4]. This is one of the utmost reasons

cancer incidences are gradually increasing every year and have become the second leading cause of death worldwide. Consequently, more than 200 types of cancer have been identified, each of which can be characterized by different molecular profiles requiring unique therapeutic strategies [1]. The most common cancers diagnosed in men are prostate, lung, and colorectal cancers, while for women, breast, lung, and colorectal cancers are most common [5].

As the importance of genetic knowledge in cancer treatment is increasingly addressed, several projects have emerged, of which The Cancer Genome Atlas (TCGA) most well-known for omics data. TCGA curates various omics data, e.g., gene mutation, gene expressions (GE), DNA methylation, CNV, and miRNA expressions. By acquiring deep insights of these data, treatment can be focused on preventive measures. Besides, clinical outcomes, i.e., clinical and pathology information are provided. TCGA further analyzed over 11,000 cancer cases from 33 prevalent forms of cancer, which fostered the accomplishment of the Pan-Cancer Atlas (PCA), which results from the normalized GE data about 20K protein-coding genes [6].

These data, however, are highly variable, high-dimensional, and sourced from heterogeneous platforms, which imposes significant challenges to existing bioinformatics tools stimulating the development of deep learning (DL)-based diagnosis and prognosis systems. Since DL algorithms work better with such high dimensional data, recent studies focused on using deep architectures such as autoencoders, CNN, and Recurrent Neural Networks (RNN). Although these models have shown tremendous success in exhibiting high confidence, they are mostly perceived as ‘black box’ methods because of a lack of understanding of their internal functioning. This is a serious drawback since interpretability is essential to generate insights on why a given cancer case is of a certain type, and since knowing the most important biomarkers can help in recommending more accurate treatments and drug repositioning. Further, the ‘right to explanation’ of the EU GDPR [7] gives patients the right to know why and how an algorithm made a diagnosis decision. However, existing approaches can neither ensure the diagnosis transparently nor are they trustworthy.

Since GE data are very high dimensional and a significant number of genes have a trivial effect on the tumor making them very weak features, we hypothesize that our approach called *OncoNetExplainer* based on neural networks (NN) and ML baselines with the explanation capability can be more effective at learning hierarchical features. We trained and

evaluated CNN and VGG16 networks with a guided-gradient class activation map (GradCAM++) [8]. Using GradCAM++, we generated heat maps (HM) for all the classes showing prominent pixels across GE values and computed the feature importance in terms of mean absolute impact (MAI) to identify important biomarkers and provide interpretations of the predictions to make the cancer diagnosis transparent. Further, we validated our findings through functional analysis to make sure the selected genes are biologically trustworthy for the corresponding tumor types. Further, SHAP is used along with GBT to validate our findings based on the annotations provided by the TumorPortal to ensure the consistency and accuracy.

The rest of the paper is structured as follows: section II discusses related works and highlights their potential limitations. Section III chronicles data collection and preparation before constructing and training the network. Section IV demonstrates some experimental results and discusses the key findings of the study. Section V provides explanations and points out the relevance of the study, highlights its limitations and discusses future works before concluding the paper.

II. RELATED WORK

Numerous approaches using genomic data, bioimaging, and clinical outcomes have been proposed for analyzing genomic profiles of patients for treatment decision making [5]. However, early detection of tumors is particularly important for better treatment of patients, a notable issue being the discrimination of tumor samples from normal ones [9]. Unlike conventional cancer typing methods that work based on morphological appearances, GE levels of the tumor are used to differentiate tumors that have similar histo-pathological appearances, giving more accurate tumor typing results for colorectal cancer diagnosis [10]. Different types of mutation data, e.g., point mutation, single nucleotide variation, INDEL, and CNV are also used. Yuan et al. [11] observed that these genomics phenomena are associated with complex diseases and contribute to the growth of different types of cancers.

Different ML algorithms were trained using mixed data types, e.g., genomic data, bioimaging data, and clinical outcomes. These approaches not only proved useful at improving cancer prognosis, diagnosis, and treatments but also revealed subtype information of several cancer types [12]. Li et al. [5] employs a genetic algorithm for feature selection and a k-nearest neighbors for the classification based on GE data from the PCA project. Their approach can classify 90% of the tumor cases correctly using different 20-gene sets. However, since the data contain GE values of more 20K protein-coding genes, these generic ML methods were found to be inefficient, with some genes appearing repeatedly in the sets because of the curse of dimensionality. Since DL algorithms work better with high dimensional data, recent studies focused on employing NN architectures, which in comparison with traditional ML-based approaches, have shown more accurate and promising results for cancer identification. In particular, CNN has shown tremendous success and has gained much attention for solving gene selection and classification based on microarray data [13].

Further, Cruz et al. [2] trained a CNN using whole slide images, and extract deep features from different cohorts, which are used to detect cancer regions. Danaee et al. [14] used a stacked denoising autoencoder to extract features from RNA-seq data, which are then fed into a SVM and a shallow ANN to classify malignant or benign tumors of breasts [15]. Although their study makes predictions on the cancer predisposition of unseen test groups of mixed DNAs with high confidence, it is limited to only Caucasian and Korean cohorts. Elsadek et al. [16] used CNVs about 23,082 genes for 2,916 instances from cBioPortal to classify the tumor samples of breast, bladder urothelial, colon, glioblastoma, kidney, and head and neck squamous cells and achieve an accuracy of 85%.

Lyu et al. [6] and Mostavi et al. [17] embedded the RNA-Seq data from the PCA project into 2D images and trained a CNN to classify 33 tumor types, which outperforms the approach in [5]. Besides, they provide a functional analysis on the genes with high intensities in the HM based on GradCAM and validated that these top genes are related to tumor-specific pathways. However, due to the stochastic nature of NN, the prediction and feature importance generated is slightly different across runs, i.e., not deterministic. This is also no exception for tree-based ensemble models such as gradient boosted trees (GBT), which provides 3 options for measuring feature importance: i) *weight*, which is the number of times a feature is used to split the data across all trees, ii) *cover*, the number of times a feature is used to split the data across all trees weighted by the number of training data points go through those splits, and iii) *gain*, which is the average training loss reduction gained when using a feature for splitting. Based on these measure, feature importance orderings (i.e., the order in which features were added) are different since subsequent features will get a disproportionately high weight.

Our proposed approach *OncoNetExplainer* first embeds high dimensional RNA-Seq data into 2D images and trains CNN and VGG16 networks with GradCAM++ activated to classify 33 tumor types based on patients' GE profiles and provides a human-interpretable explanation (post-model explainability) to identify important biomarkers, which is further validated based on the annotations from TumorPortal. To provide a comparison with baselines, we also identify the top-K biomarkers for each cancer type and cancer specific driver genes based on GBT and SHAP (pre-model explainability).

III. MATERIALS AND METHODS

In this section, we discuss the data preparation, network construction, training, and biomarkers discovery with ranking.

A. Data collection and preparation

We use the cancer transcriptomes from the Pan-Cancer Atlas project to interrogate GE states induced by deleterious mutations and copy number alterations. In particular, GE profiles about 33 prevalent tumor type for 9,074 samples are used in our approach. This dataset has been used widely as prior knowledge to generate tumor-specific biomarkers [18–20]. These data are hybridized by the Affymetrix 6.0, which

allows us to examine the largest number of cases along with the highest probe density [21]. Table I shows sample distribution. To apply the convolutional (conv) operations,

TABLE I: Sample distribution across different tumor types

Cohort	#Sample	Carcinoma type
BRCA	981	Breast invasive carcinoma
LGG	507	Brain lower grade glioma
UCEC	507	Uterine endometrial carcinoma
LUAD	502	Lung adeno-carcinoma
HNSC	487	Head-neck squamous cell carcinoma
THCA	480	Thyroid carcinoma
PRAD	479	Prostate adeno-carcinoma
LUSC	464	Lung squamous cell carcinoma
BLCA	398	Bladder urothelial carcinoma
STAD	383	Stomach adeno-carcinoma
SKCM	363	Skin cutaneous melanoma
KIRC	352	Kidney renal clear cellcarcinoma
LIHC	348	Liver hepato-cellular carcinoma
COAD	341	Colon adeno-carcinoma
CESC	272	Cervical & endo-cervical cancer
KIRP	271	Kidney papillary cell carcinoma
SARC	229	Sarcoma
OV	176	Ovarian serouscystadenocarcinoma
ESCA	169	Esophageal carcinoma
PCPG	161	Pheochromocytoma-paraganglioma
PAAD	152	Pancreatic adenocarcinoma
TGCT	144	Testicular germ cell tumor
GBM	124	Glioblastoma multiforme
THYM	119	Thymoma
READ	118	Rectum adeno-carcinoma
LAML	115	Acute myeloid leukemia
MESO	82	Mesothelioma
UVM	80	Uveal melanoma
ACC	76	Adrenocortical cancer
KICH	65	Kidney chromophobe
UCS	56	Uterine carcino-sarcoma
DLBC	37	Diffuse large B-cell lymphoma
CHOL	36	Cholangio carcinoma

we embed GE samples into 2D images in which GE values for each sample are reshaped from a $20,501 \times 1$ array into a 144×144 image by zero padding around the edges and normalized to $[0,255]$ without losing any information.

B. Network construction and training

We trained a shallow CNN from scratch alongside data augmentation in which the output of each conv layer is passed to dropout and Gaussian noise layers to avoid overfitting and thus regularize the learning [22]. This involves the input feature space into a lower-dimensional representation, which is then further down-sampled by two different pooling layers and a max-pooling layer (MPL) by setting the pool size. The output of an MPL is considered as an ‘extracted feature’ from each 2D GE image. Since each MPL ‘flattens’ the output space by taking the highest value in a FM, this produces a sequence vector from the last conv layer, which we expect to force the GE value of specific genes that are highly indicative of being responsible for a specific cancer type. Then this vector is passed through another dropout layer and a fully connected softmax for the probability distribution over the classes.

The CNN is trained with AdaGrad to optimize the categorical cross-entropy loss of the predicted cancer type vs. actual cancer type. Further, we observe the performance by adding the Gaussian noise layer (GNL) following each conv layer to improve model generalization. Further, we used the pretrained VGG16 network to which we added two dense layers at the

end of the original architecture, followed by a GNL. Then, we fine-tuned the top layers with minor weight updates:

- First, we instantiated the conv base of the VGG16 network and loaded its weights.
- Then, we added our previously defined fully-connected layers on top with minor weight updates.
- Finally, we placed a softmax layer by freezing up to the last conv block of the VGG16 model, which yields a probability distribution over 33 different classes.

Since the data is very high dimensional, we chose not to go for manual feature selection. Rather, we let both CNN and VGG16 networks extract the most important features. The guided back-propagation helps to generate more human-interpretable but fewer class-sensitive visualizations than the saliency maps (SM) [23]. Since SM use true gradients, the trained weights are likely to impose a stronger bias towards specific subsets of the input pixels. Accordingly, class-relevant pixels are highlighted rather than producing random noise [23]. Therefore, GradCAM++ is used to draw the HM to provide attention to most important genes. Class-specific weights of each FM are collected from the final conv layer through globally averaged gradients (GAG) of FMs instead of pooling [8]:

$$\alpha_k^c = \frac{1}{Z} \sum_i \sum_j \frac{\partial y^c}{\partial A_{ij}^k} \quad (1)$$

where Z is the number of pixels in a FM, c is the gradient of the class, and A_{ij}^k is the value of k th FM at (i, j) . Having gathered relative weights, the coarse SM, L^c is computed as the weighted sum of $\alpha_k^c * A_{ij}^k$ of the ReLU activation function and employ the linear combination to the FM, since only the features with positive influence on the class are of interest [8].

$$L^c = \text{ReLU}\left(\sum_i \alpha_k^c A^k\right) \quad (2)$$

The GradCAM++ replaces the GAG with a weighted average of the pixel-wise gradients (eq. (3)), since the weights of pixels contribute to the final prediction (eq. (4)) by aggregating eq. (3) and α_{ij}^{kc} (eq. (5)). In summary, it applies the following iterators over the same activation map A^k , (i, j) and (a, b) :

$$w_k^c = \sum_i \sum_j \alpha_{ij}^{kc} \cdot \text{ReLU}\left(\frac{\partial y^c}{\partial A_{ij}^k}\right) \quad (3)$$

$$y^c = \sum_k w_k^c \cdot \sum_i \sum_j A_{ij}^k \quad (4)$$

$$\alpha_{ij}^{kc} = \frac{\frac{\partial^2 y^c}{(\partial A_{ij}^k)^2}}{2 \frac{\partial^2 y^c}{(\partial A_{ij}^k)^2} + \sum_a \sum_b A_{ab}^k \frac{\partial^3 y^c}{\{(\partial A_{ij}^k)^3\}}} \quad (5)$$

Further, since an appropriate selection of hyperparameters can have a huge impact on the performance of a deep architecture, we perform the hyperparameter optimization through a random search and 5-fold cross-validation tests. In each of 5 runs, 70% of the data is used for the training, 30% for the evaluation. 10% of the training set is used for validation of the networks to optimize the cross-entropy loss based on the best learning rate, batch size, number of filters, kernel size, and dropout/Gaussian noise probability.

Algorithm 1: Computing feature importance and ranking genes

Input : 2D GE images $\mathcal{D} = (d_1, d_2, \dots, d_n)$ having ground truth (i.e., labels) $\mathcal{L} = (l_1, l_2, \dots, l_j)$ on which a CNN model is trained for each fold $\mathcal{M} = (m_1, m_2, \dots, m_i)$ to find k for top-k genes that satisfy MAI threshold.

Output: feature importance $\mathcal{F} = (f_1, i_1)(f_2, i_2), \dots, (f_n, i_n)$ and top features \mathcal{T} across all images per fold per class.

```
for fold  $\in$  FOLDS do
   $\mathcal{P} \leftarrow \{\}$  // Guided backprop for each image per fold per class
   $\mathcal{K} \leftarrow \{\}$  // GradCAM++(GCAM) for all images per fold per class
   $\mathcal{I} \leftarrow \{\}$  // GCAM of each image in a fold
   $\mathcal{G} \leftarrow \{\}$  // GCAM for all images per fold per class
   $\mathcal{F} \leftarrow \{\}$  // Feature importance of each gene per class per fold
   $\mathcal{T} \leftarrow \{\}$  // Top genes and importance per class per fold
  for  $d \in \mathcal{D}$  do
     $\mathcal{K} \leftarrow \text{gradCAM}++(m_d, d, l_d)$  // GCAM of images per fold per class
     $\mathcal{P} \leftarrow \text{guidedBackprop}(m_d, d)$  // Guided backprop of each image
     $\mathcal{I} \leftarrow \mathcal{K} * \mathcal{P}$  // GCAM of each image
     $\mathcal{G} \leftarrow \mathcal{G} \cup \mathcal{I}$  // GCAM for all the images in fold
   $\mathcal{F} \leftarrow \frac{1}{N} \sum_{i=1}^N \mathcal{G}$  // Mean absolute impact for genes for axis=0
  if  $F_i < \sigma$  then // If the feature importance is less than MAI
     $\mathcal{F} \leftarrow \mathcal{F} - F_i$  // Pop off insignificant genes
     $\mathcal{T} \leftarrow \text{sort}_k(\mathcal{F})$  // Sort and choose top genes based on MAI
  Return  $\mathcal{F}, \mathcal{T}$ 
```

Algorithm 2: Identification of important areas

Input : importance of current class across folds $\mathcal{F} = (f_1, \dots, f_i)$, height h & width w of rectangle, & MAI threshold σ .

Output: important areas $\mathcal{C} = (x_1, y_1), (x_2, y_2), \dots, (x_n, y_n)$ in an image per fold.

```
for fold  $\in$  FOLDS do
   $\mathcal{A} \leftarrow \text{dict}()$  // Importance of areas
   $\mathcal{S} \leftarrow \text{list}()$  // Sorted areas by MAI
   $\mathcal{C} \leftarrow \text{list}()$  // Important areas
  for  $h$  do
    for  $w$  do
       $\text{area} \leftarrow \mathcal{F}[h : h + \text{shape}[0], w : w + \text{shape}[1]]$  // Area of image
       $\text{impA} \leftarrow 0$  // Importance of current area in the image
      for  $\text{row} \in \text{area}$  do
        for  $\text{imp} \in \text{row}$  do
          if  $\text{imp} > \sigma$  then // If feature importance is greater than MAI
             $\text{impA} += \text{imp} - \sigma$  // Importance of area = current importance - MAI
           $\mathcal{A}[\text{area}] = \text{impA}$  // We update the importance of the area
   $\mathcal{S} \leftarrow \text{sort}(\mathcal{A}, \text{reverse} = \text{true})$ 
  for  $a, i \in \mathcal{S}$  do
    if  $a \cap i = \text{then}$  // Non-intersecting area with important areas
       $\mathcal{C} \leftarrow \mathcal{C} \cup a$  // It's a new important area added to the list
  Return  $\mathcal{C}$ 
```

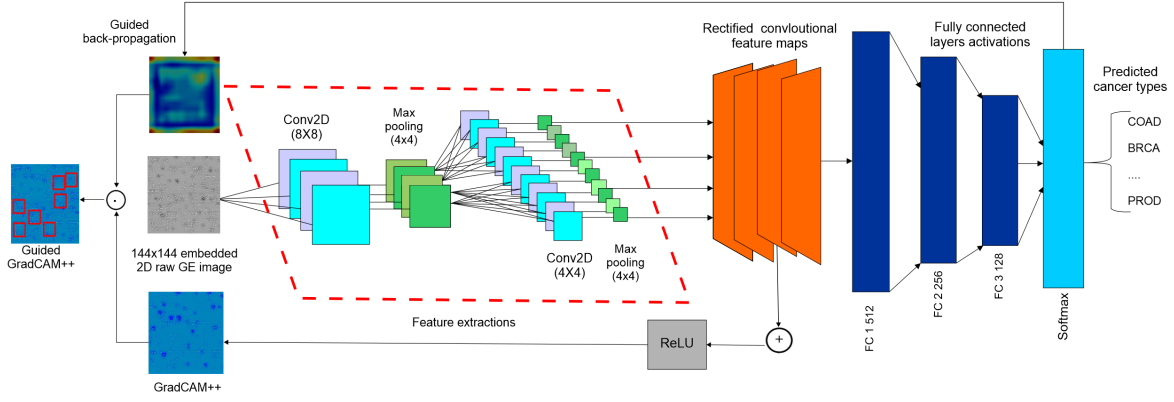


Fig. 1: Schematic representation of our approach, which starts from taking a raw GE sample and passing to conv layers before obtaining rectified conv feature maps (with guided-backprop & GradCAM++) to pass through dense, dropout, & softmax layer

C. Finding and validating important biomarkers

Algorithm 1 and 2 depict the pseudocodes for computing feature importance with ranking genes and identification of important areas on the HM, respectively. We averaged all the normalized HM from the same class to generate a class-specific HM inspired by Selvaraju et al. [8]. In the HM, a higher intensity pixel represents a higher significance to the final prediction, which indicates higher importance of corresponding genes and the GE values. Top genes are then selected based on the intensity rankings and MAI threshold. Since GradCAM++ requires all the samples to run through the network once, we let the trained CNN models set and record the activation maps in the forward pass, and the gradient maps in the back-prop to collect the HM for each sample.

In contrast, Shapley values are used to calculate the importance of a feature by comparing what a model predicts with and without a feature from all possible combinations of n features in the dataset S . Given a GE value of feature $i \in S$, SHAP calculates the prediction p of the model with i . The Shapley value ϕ is calculated as follows [24]:

$$\phi_i(p) = \sum_{S \subseteq N/i} \frac{|S|!(n - |S| - 1)!}{n!} (p(S \cup i) - p(S)) \quad (6)$$

However, since the order in which a model sees features can affect the predictions, this computation is repeated in all possible orders to compare the features fairly. Feature that have no effect on the predicted value are expected to produce a Shapley value of 0. However, if two features contribute equally to the prediction, the Shapley values should be the same [24].

IV. EXPERIMENTS

Implementation was done in Python¹ using a software stack comprising Scikit-learn and Keras with the TensorFlow backend. The network was trained on an Nvidia GTX 1080i GPU with CUDA and cuDNN enabled. Results based on hyperparameters produced through random search and 5-fold cross-validation are reported and discussed with a comparative analysis with macro-averaged precision and recall. Further,

since the classes are imbalanced, Matthias correlation coefficient (MCC) scores were reported. Since it is important for cancer diagnosis to have both high precision and high recall [25], results with very different precision and recall are not useful in cancer diagnosing and tumor type identification. Hence, we did not report F1-scores.

A. Performance of cancer type classification

The average accuracy obtained was 89.75% and 96.25% using CNN and VGG16 models, respectively. However, since the classes are imbalanced, only the accuracy will give a very distorted estimation of the cancer types. Thus, we report the class-specific classification reports along with the corresponding MCC scores in table II. As can be seen, precision and recall for the majority cancer types were high and for these the VGG16 model performs mostly better. Notably, the VGG16 model classifies BRCA, UCEC, LUAD, HNSC, LUSC, THCA, PRAD, BLCA, STAD, KIRC, LIHC, COAD, CESC, KIRP, SARC, OV, PCPG, TGCT, GBM, READ, LAML, MESO, and DLBC cancer cases more confidently, whereas the CNN model classifies PAAD, CHOL, and UCS cancer cases more accurately.

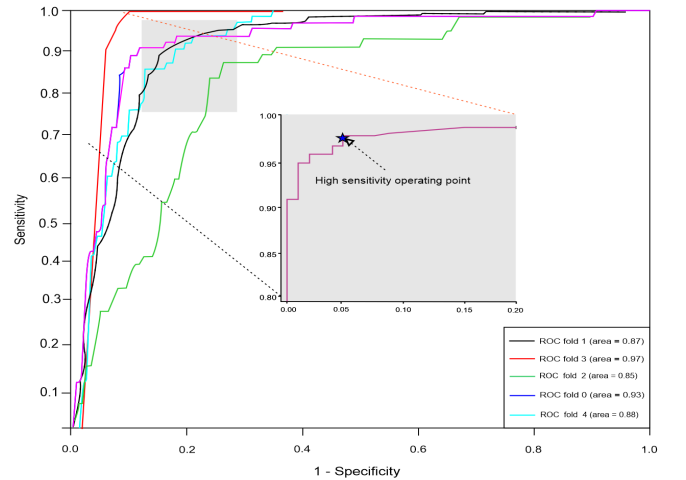


Fig. 2: ROC curves of the VGG16 model across folds

The ROC curves generated by the VGG16 model in fig. 2 show that the AUC scores are consistent across the folds. This

¹ https://github.com/rezacsedu/XAI_Cancer_Prediction

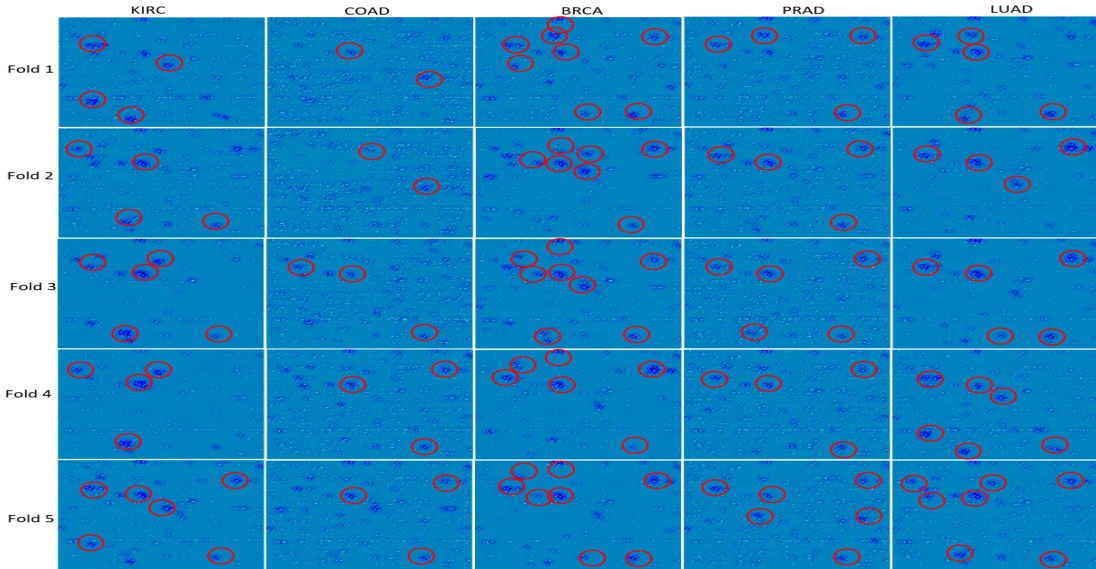


Fig. 3: Heat map examples for selected cancer types. Each row represents the result from one fold. Columns represent the heat maps of BRCA, KIRC, COAD, LUAD, and PRAD cancer types (patterns are not clearly visible in some folds, though)

TABLE II: Cancer type prediction: CNN vs VGG16

Type	CNN (89.75%)			VGG16 (96.25%)		
	Precision	Recall	MCC	Precision	Recall	MCC
BRCA	0.8785	0.8612	0.7564	0.9437	0.9511	0.8465
LGG	0.9254	0.8926	0.8330	0.9311	0.9402	0.8421
UCEC	0.8753	0.8819	0.7835	0.9562	0.9429	0.8445
LUAD	0.8235	0.8354	0.7136	0.9865	0.9823	0.8624
HNSC	0.8520	0.8743	0.7851	0.9730	0.9822	0.8765
THCA	0.8528	0.8323	0.7275	0.9138	0.9154	0.8125
PRAD	0.8827	0.8778	0.7847	0.9233	0.9347	0.8207
LUSC	0.8726	0.8634	0.7625	0.9434	0.9472	0.8524
BLCA	0.8956	0.9037	0.8075	0.9656	0.9537	0.8475
STAD	0.8253	0.8156	0.6932	0.9653	0.9556	0.8532
SKCM	0.8853	0.8711	0.8025	0.9046	0.9136	0.8168
KIRC	0.8967	0.9123	0.8237	0.9578	0.9689	0.8531
LIHC	0.8194	0.8085	0.6945	0.9572	0.9664	0.8537
COAD	0.8368	0.8245	0.7679	0.9776	0.9690	0.8514
CESC	0.8785	0.8743	0.7964	0.9873	0.9885	0.8664
KIRP	0.8254	0.8032	0.7043	0.9681	0.9782	0.8430
SARC	0.8753	0.8671	0.7835	0.9365	0.9435	0.8421
OV	0.8825	0.8733	0.7936	0.9725	0.9773	0.8262
ESCA	0.8913	0.8719	0.7951	0.8956	0.8834	0.8076
PCPG	0.8537	0.8611	0.7875	0.9875	0.9987	0.8735
PAAD	0.9629	0.9567	0.8407	0.9452	0.9500	0.8325
TGCT	0.8736	0.8722	0.7825	0.9890	0.9724	0.8434
GBM	0.8952	0.8845	0.8075	0.9362	0.9453	0.8436
THYM	0.9255	0.9123	0.8232	0.9775	0.9678	0.8622
READ	0.6795	0.6857	0.6225	0.8874	0.8733	0.7525
LAML	0.8697	0.8567	0.8237	0.9576	0.9632	0.8513
MESO	0.8991	0.9028	0.8076	0.9534	0.9456	0.8457
UVM	0.8765	0.8623	0.7979	0.9136	0.9089	0.8184
ACC	0.9217	0.9345	0.8225	0.9623	0.9731	0.8611
KICH	0.9335	0.9475	0.8425	0.9690	0.9625	0.8439
UCS	0.9157	0.9064	0.8125	0.8726	0.8675	0.7869
DLBC	0.8678	0.8729	0.7005	0.9347	0.9421	0.8389
CHOL	0.8838	0.8975	0.7979	0.8455	0.8342	0.6821
Average	0.8975	0.9065	0.8052	0.9625	0.9542	0.8453

signifies that the predictions by the VGG16 model are much better than random guessing. Further, the class-specific MCC scores of the VGG16 model is 4% higher than that of the CNN model, which suggests that the predictions were strongly correlated with the ground truth, yielding a Pearson product-moment correlation coefficient higher than 0.70 for all the classes except for the CHOL tumor samples. The downside, however, is that both classifiers made a number of mistakes

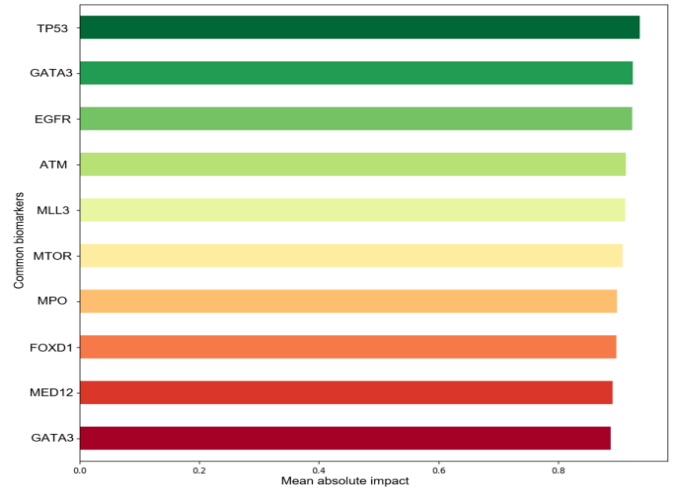


Fig. 4: Common driver genes across 33 cancer types)

too, e.g., VGG16 can classify ESCA, READ, UCS, and CHOL tumor cases in only 89% of the cases accurately, while the CNN model made more mistakes particularly for the READ, LUAD, LIHC, KIRP, COAD, and STAD tumor samples.

B. Feature importance and validation of top biomarkers

We identified top genes for which the change in expression has significant impact on patients. Figure 3 shows examples of HM generated for each class across 5 different folds. As seen, there are similarities across folds and displaying distinct and similar patterns when comparing different cancer types. The red circles highlight similar patterns, e.g., between KIRC and BRCA, and PRAD and LUAD across folds, whereas COAD shows very different patterns. Although there are differences among folds, some patterns are clearly visible. Since intensities did not follow any regular pattern, we chose top 660 genes across 33 tumor types (top-20 genes per class) as

TABLE III: Top-5 genes and their importance

Type	Gene	Gene type	MAI
BRCA	TP53	Oncogene	0.78125
	GATA3	Protein-coding	0.760784
	MLL3	Protein-coding	0.664706
	TBX3	Oncogene	0.574118
	MPO	Protein-coding	0.538039
KIRC	MTOR	Oncogene	0.596078
	SETD2	Protein-coding	0.560784
	ATM	Protein-coding	0.540784
	MPO	Oncogene	0.531569
	AMBN	Oncogene	0.523137
LUAD	EGFR	Oncogene	0.860000
	KEAP1	Protein-coding	0.820784
	ERBB2	Oncogene	0.764706
	MLL3	Protein-coding	0.674118
	AMBN	Protein-coding	0.558039
PRAD	FOXA1	Oncogene	0.556078
	TP53	Oncogene	0.520784
	ATM	Protein-coding	0.510784
	AMBN	Protein-coding	0.491569
	MED12	Protein-coding	0.453137
COAD	EPHA6	Protein-coding	0.756078
	TIMP1	Protein-coding	0.720784
	ART5	Protein-coding	0.680784
	FOXD1	Protein-coding	0.661569
	AMBN	Protein-coding	0.563137

more significant based on the measure of MAI. Since we have more than 20K protein-coding genes, our choice of 660 is still a reasonable choice, since the number of important biomarkers should be small whose GE changes are sensitive to cancer growth [3]. All genes in the top-20 list can thus be viewed as tumor-specific biomarkers, which contribute most toward making the predictions. As for the other 29 tumor types, only 3 genes were in the list. Further hyperparameter tuning and training of both CNN models might improve this outcome.

Then we further narrowed down the list to the top-5 genes in which only 5 tumor types (i.e., BRCA, KIRC, COAD, LUAD, and PRAD) have at least five genes with feature importance of at least 0.5 w.r.t. MAI; they are shown in table III. To further validate our findings, the saturation analyses of cancer genes across 33 tumor types (except for COAD) are obtained from the TumorPortal [26]. Validation for the COAD cancer follows a signature-based approach [3], which was used for predicting the progression of colorectal cancer. However, our approach makes some false identifications, as 21 out of 25 genes are validated to be correct, making only 4 false identifications.

C. Finding common biomarkers

Identifying all significant common genes will help understand various aspects for a specific cancer type (e.g., BRCA carcinogenesis). Thus, these top genes have close relations to the corresponding tumor types, which could be viewed as potential biomarkers. Figure 4 shows the top-10 common biomarkers, in which KRTAP1-1, INPP5K, GAS8, MC1R, POLR2A, BET1P1, NAT2, PSD3, KAT6A, and INTS10 genes are common across cancer types, with the INTS protein-coding gene having the highest feature importance of 0.6.

D. Explanations with SHAP

The GBT model is trained to provide explanations generated by SHAP. Figure 5 shows a base value that indicates the

direction of the first prediction made by the GBT model and shows how much each feature is pushing the model’s output from the base value² 0.55 to the predicted output. Features pushing the prediction higher are shown in red; those pushing the prediction lower are in blue. Further, to get an overview of which biomarkers are most important for the GBT model, we plot the SHAP values of each feature for each sample. The plot in fig. 6 sorts features by the sum of SHAP value magnitudes over all the samples, shows the distribution of the impact of each feature on the model output, and gives the top-20 common biomarkers, where red represents high feature values, blue low. This reveals, e.g., that a low NACA2 (low GE value) lowers the predicted value. Since the common biomarkers predicted by VGG16 (fig. 4) and GBT (fig. 6) are very different, a more detailed analysis of biological signaling pathways is further required to validate these findings.

E. Comparison with related works

OncoNetExplainer slightly outperforms the approach by Boyu et al. [6] but 6.5% better than the approach by Yuanyuan et al. [5]. Further, *OncoNetExplainer* can improve the false prediction rate for the READ, UCS, ESCA, and CHOL tumor samples. In particular, against 35%, 81%, 77%, and 56% of the correctly predicted cases by [6], our approach can predict 88.74%, 87.26%, 89.56%, and 84.55% (in cyan) of the same cases correctly. Although *OncoNetExplainer* performs slightly worse than [6] at classifying BRCA, THCA, and PRAD (in red), it is more consistent for the majority of cancer types and likely to perform more stably on new GE data. *OncoNetExplainer* provides both pre-model (GBT) and post-model interpretation (CNN and VGG16), whereas [6] provides only the post-model interpretability. Some other studies also used GE data [16,27] for the cancer prediction. However, since GE data from the PCA project had more samples, a one-to-one comparison with these studies was not viable.

V. CONCLUSION AND OUTLOOK

In this paper, we proposed *OncoNetExplainer*, an explainable method for the prediction of cancer types based on GE data. Our approach is based on GradCAM++ with CNN and VGG16 networks, and SHAP-based GBT model. Experiment results show that GE is useful for predicting cancer types with high confidence giving an accuracy of up to 96.25%. We also attempted to provide a more human-interpretable explanation by showing statistically significant biomarkers. These analyses are further validated with scientific literature [26], which confirms that the identified genes are biologically relevant.

Although we attempted to open the CNN and VGG16 black-box models through biomarker validation and feature ranking, our approach is mostly post-hoc in that the explainability is based on test cases and results similar to layer-wise relevance propagation. Several further factors have hindered this research: i) lack of enough training samples, ii) lack of biological pathways analysis, and iii) since multiple factors are involved in cancer diagnosis (e.g., estrogen, progesterone, and

² The average model output over the training dataset passed



Fig. 5: Clinical features' contribution for the first prediction: pushing the prediction higher and lower in red and blue, respectively

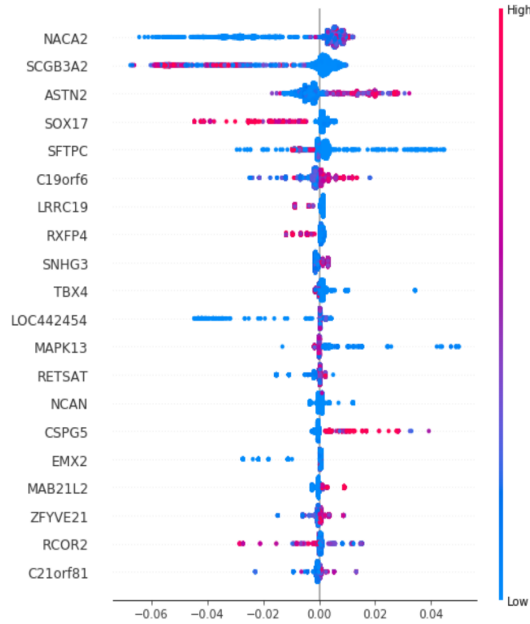


Fig. 6: Clinical features ordered by ascending importance on the y-axis (dots represent SHAP values of specific features)

epidermal growth receptors in BRCA), AI-based diagnoses might not be trustworthy solely based on a single modality, which demands the requirements of multimodal features of DNA methylation, GE, miRNA expression, and CNVs data.

In the future, we intend to extend this work by: i) alleviating more samples by combining genomics data from ICGC and COSMIC to train a multimodal architecture, ii) improving the explanations about the predictions using an ante-hoc approach by seeding explainability into the model from the beginning. In particular, we will focus on multimodality with reversed time attention model and Bayesian deep learning [28].

REFERENCES

- [1] K. Tomczak, P. Czerwińska, and M. Wiznerowicz, "The cancer genome atlas (TCGA): an immeasurable source of knowledge," *Contemporary oncology*, vol. 19(1A), p. A68, 2015.
- [2] A. Cruz-Roa *et al.*, "Accurate and reproducible invasive breast cancer detection in whole-slide images: A deep learning approach for quantifying tumor extent," *Scientific Reports*, vol. 7, p. 46450, 2017.
- [3] S. Zuo, G. Dai, and X. Ren, "Identification of a 6-gene signature predicting prognosis for colorectal cancer," *Cancer cell international*, vol. 19, no. 1, p. 6, 2019.
- [4] M. D. Podolsky and *et al.*, "Evaluation of machine learning algorithm utilization for lung cancer classification based on gene expression levels," *Journal of Cancer Prevention*, vol. 17(2), pp. 835–838, 2016.
- [5] Y. Li, K. Kang, J. Krahn, and L. Li, "A comprehensive genomic pan-cancer classification using the cancer genome atlas gene expression data," *BMC genomics*, vol. 18, no. 1, p. 508, 2017.
- [6] B. Lyu and A. Haque, "Deep learning based tumor type classification using gene expression," in *Pro. of ACM Intl. Conf. on Bioinformatics, Computational Biology, & Health Informatics*. ACM, 2018, pp. 89–96.
- [7] M. E. Kaminski, "The right to explanation, explained," *Berkeley Tech. LJ*, vol. 34, p. 189, 2019.

- [8] A. Chattopadhyay and A. Sarkar, "Grad-CAM++: Generalized gradient-based visual explanations for deep convolutional networks," in *Conf. on Applications of Computer Vision (WACV)*. IEEE, 2018, pp. 839–847.
- [9] J. Liu, X. Wang, Y. Cheng, and L. Zhang, "Tumor gene expression data classification via sample expansion-based deep learning," *Oncotarget*, vol. 8, no. 65, p. 109646, 2017.
- [10] V. Paroder, S. R. Spencer, M. Paroder, D. Arango, and N. Carrasco, "Na+/monocarboxylate transport (SMCT) protein expression correlates with survival in colon cancer," *Proceedings of the National Academy of Sciences*, vol. 103, no. 19, pp. 7270–7275, 2006.
- [11] Y. Yuan, Y. Shi, X. Su, and Z.-G. Han, "Cancer type prediction based on copy number aberration and chromatin 3d structure with convolutional neural networks," *BMC genomics*, vol. 19, no. 6, p. 97, 2018.
- [12] L. Huang and *et al.*, "Copy number variation at 6q13 functions as a long-range regulator and is associated with pancreatic cancer risk," *Carcinogenesis*, vol. 33(1), pp. 94–100, 2011.
- [13] D. Q. Zeebaree, H. Haron, and A. M. Abdulazeez, "Gene selection & classification of microarray data using convolutional neural network," in *Intl. Conf. on Advanced Science & Eng.* IEEE, 2018, pp. 145–150.
- [14] P. Danaee, R. Ghaeini, and D. A. Hendrix, "A deep learning approach for cancer detection and relevant gene identification," *Pacific Symposium on Biocomputing*, vol. 22, p. NIH Public Access, 2016.
- [15] H. Chen, "Supervised machine learning for high dimensional gene data in colon cancer detection," *IEEE Intl. Congress on Big Data*, 2015.
- [16] S. F. A. Elsadek, M. A. A. Makhlof, and M. A. Aldeen, "Supervised classification of cancers based on CNVs," in *Intl. Conf. on Advanced Intelligent Systems & Informatics*. Springer, 2018, pp. 198–207.
- [17] M. Mostavi, Y. Chiu, and Y. Chen, "Convolutional neural network for cancer type prediction using gene expression," *arXiv:1906.07794*, 2019.
- [18] G. P. Way, F. Sanchez-Vega, K. La, J. Armenia, W. K. Chatila, A. Luna, C. Sander, A. D. Cherniack, M. Mina, G. Ciriello *et al.*, "Machine learning detects pan-cancer ras pathway activation in the cancer genome atlas," *Cell reports*, vol. 23, no. 1, pp. 172–180, 2018.
- [19] K. A. Hoadley, C. Yau, T. Hinoue, D. M. Wolf, A. J. Lazar, E. Drill, R. Shen, A. M. Taylor, A. D. Cherniack, V. Thorsson *et al.*, "Cell-of-origin patterns dominate the molecular classification of 10,000 tumors from 33 types of cancer," *Cell*, vol. 173, no. 2, pp. 291–304, 2018.
- [20] T. M. Malta, A. Sokolov, A. J. Gentles, T. Burzykowski, L. Poisson, J. N. Weinstein, B. Kamińska, M. Huelsken, L. Omberg, O. Gevaert *et al.*, "Machine learning identifies stemness features associated with oncogenic dedifferentiation," *Cell*, vol. 173, no. 2, pp. 338–354, 2018.
- [21] R. W. Park, "Identification of rare germline copy number variations in five human cancer types," *Molecular cancer*, vol. 14(1), p. 25, 2015.
- [22] D. P. Kingma and M. Welling, "Variational dropout and the local reparameterization trick," in *NeuralIPS*, 2015, pp. 2575–2583.
- [23] W. Nie and A. Patel, "A theoretical explanation for perplexing behaviors of backpropagation-based visualizations," *arXiv:1805.07039*, 2018.
- [24] S. M. Lundberg and S.-I. Lee, "A unified approach to interpreting model predictions," in *Advances in Neural Information Processing Systems*. Curran Associates, Inc., 2017, pp. 4765–4774.
- [25] S. Naulaerts, C. C. Dang, and P. J. Ballester, "Precision and recall oncology: combining multiple gene mutations for improved identification of drug-sensitive tumours," *Oncotarget*, vol. 8, no. 57, p. 97025, 2017.
- [26] M. S. Lawrence, P. Stojanov, C. H. Mermel, J. T. Robinson, L. A. Garraway, T. R. Golub, M. Meyerson, S. B. Gabriel, E. S. Lander, and G. Getz, "Discovery and saturation analysis of cancer genes across 21 tumour types," *Nature*, vol. 505, no. 7484, p. 495, 2014.
- [27] N. Zhang, M. Wang, P. Zhang, and T. Huang, "Classification of cancers based on copy number variation landscapes," *Biochimica et Biophysica Acta (BBA)-General Subjects*, vol. 1860, no. 11, pp. 2750–2755, 2016.
- [28] E. Choi and W. Stewart, "Retain: An interpretable predictive model for healthcare using reverse time attention mechanism," in *Advances in Neural Information Processing Systems*, 2016, pp. 3504–3512.